Available online at www.sciencedirect.com

ScienceDirect

journal homepage: www.elsevier.com/locate/he

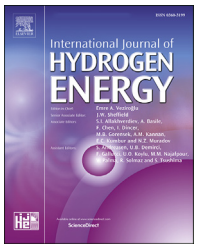

Unstretched unburned flame speed and burned gas Markstein length of diluted hydrogen/air mixtures

Berk Can Duva[*], *Elisa Toulson*

Alternative Fuels and Combustion Laboratory, Department of Mechanical Engineering, Michigan State University East Lansing, MI, USA

HIGHLIGHTS

- The S_u^o and L_b of diluted H_2/air flames are examined at 1–2 bar, 373–473 K, and $\varphi = 0.7$.
- The S_u^o increases with T due to boosted dissociation reactions and greater expansion ratios.
- The S_u^o decreases with P primarily because of reduced active radicals.
- The S_u^o drops almost linearly with dilution due to the low chemical reactivity of the diluent.
- $H + O_2 + M \leftrightarrow HO_2 + M$ and $H + OH + M \leftrightarrow H_2O + M$ are mainly responsible for the chemical effect of the diluent.

ARTICLE INFO

Article history:
Received 10 October 2021
Received in revised form
22 December 2021
Accepted 23 December 2021
Available online 20 January 2022

Keywords:
Laminar burning velocity
Markstein length
Flame speed
Hydrogen
Dilution

ABSTRACT

Fundamental combustion characteristics of H_2/air flames with the addition of actual H_2/air combustion residuals (a mixture of 65% N_2 + 35% H_2O by mole) are examined experimentally and numerically at 1–2 bar, 373–473 K, equivalence ratio of 0.7, and dilution ratios of 0–40%. Spherically expanding flame measurements at constant pressure show that flame speed and adiabatic flame temperature drop almost linearly with increasing diluent level. Detailed numerical simulations and analyses of sensitivity coefficients reveal that this is because of the low chemical reactivity of the dilution mixture. On the other hand, the change in burned gas Markstein length with the dilution mixture addition is found more complex and cannot be represented with a linear trend. Experimental flame speed data are compared with results of chemical kinetic analyses obtained by several chemical mechanisms in order to assess the accuracy of these models.

Introduction

Strict NO_x and CO emission standards have led gas turbine engine manufacturers to concentrate on constant pressure sequential combustion systems [1], or axial stage combustion concepts [2], as axial fuel staging provides significant emissions, fuel, and operational flexibilities [1–4]. Therefore, in addition to their air quality benefits, staged combustion systems facilitate overcoming the grid stability problems due to the intermittent nature of increasing solar and wind power productions and contribute to fuel diversity and energy security [5,6].

The essential feature of sequential two-stage combustors is that combustion takes place in two successive stages in series at nearly the same pressure, namely a primary burner

* *Corresponding author.*
E-mail address: duvaberk@msu.edu (B.C. Duva).
https://doi.org/10.1016/j.ijhydene.2021.12.217

system (first stage) and a secondary burner system (second stage) [1]. The primary burner flame is a conventional (usually swirled) lean turbulent premixed flame [7]. In the secondary stage, combustion occurs at high temperatures and reduced oxygen concentrations because of hot gases produced by the lean flame of the first stage, which enables low NO_x operation and combined cycle efficiency improvements [4,6,7]. Moreover, injection of a portion of the fuel or fuel/air mixture into the secondary stage reduces the residence time for the overall flow, which lowers emissions [2]. In fact, staged combustion systems were demonstrated to have the potential of a 10–40% reduction in NO_x emissions [8]. Similarly, with a perfect mixing assumption, Goh et al. [9] showed that sequential two-stage combustors can decrease NO_x emissions to one-fiftieth of the NO_x emission level of conventional dry low NO_x-type combustors. However, hot (mostly inert) combustion residuals passing onto the secondary stage from the primary stage change the flame reactivity, flame stability, and combustion stability in the secondary burner system [10].

Driven by global warming, gas turbine engine manufacturers have started to focus on carbon-free thermal power cycles. Hydrogen (H_2) has become a promising alternative to conventional ground-based power gas turbine fuels, such as natural gas, due to its high calorific value [11]. Using excessive renewable energy to produce it, i.e. Power-to-Gas, H_2 has the potential to store energy for medium to long storage cycles [12]. Therefore, the gas turbine industry committed to achieve 100% H_2 firing, i.e. a carbon neutral energy system, by 2030 [13].

The axial (sequential) stage combustion systems play an important role in 100% H_2 firing because conventional combustors fail to handle this operation in premixed mode without compromising performance [12]. However, H_2 is very reactive compared to natural gas, which results in high flame speeds/burning velocities and very fast chemical times [11]. There is a risk of the flame moving upstream and causing static instabilities, such as flashback within the burner [3,12]. Consequently, it is imperative to investigate the flame reactivity, flame stability, and combustion stability for H_2/air flames and changes in these combustion characteristics in the secondary burner system with the introduction of post combustion products coming from the primary burner system.

The reactivity, exothermicity, and essential flame/combustion stability characteristics, such as blowoff, blowout, flashback, and liftoff, of a combustible mixture are associated with the unstretched unburned flame speed (S_u^o) and burned gas Markstein length (L_b) [14–16]. Additionally, the S_u^o is frequently used to develop, optimize, and validate chemical mechanisms [17] and to predict the turbulent flame speed within a gas turbine as several combustion models are built on the S_u^o [15]. Therefore, the S_u^o and L_b are critical burner design parameters and extensive effort has been made to experimentally investigate the S_u^o and L_b of diluted H_2/oxidizer flames over the years.

Replacement of nitrogen (N_2) in the air with helium (He) and/or argon (Ar), i.e. the He/Ar dilution, is a common technique to sustain a stable H_2 flame for flame speed measurements, for instance Refs. [18–20]. One of the earliest studies investigating the dilution effect of one of the main exhaust gases of H_2/air combustion, i.e. N_2 and water vapor (H_2O), was published by Liu and MacFarlane [21] who measured burning velocities of H_2/air mixtures diluted with steam by up to 15% by volume at 1 bar and 296–523 K. Koroll and Mulpuru [22] employed the cone angle method in a nozzle burner to compare the effects of various diluents, namely He, Ar, N_2, and H_2O, on the burning velocity of H_2/O_2 mixtures at 1 bar and 298–373 K.

Aung et al. [23] examined effects of positive flame stretch on the laminar burning velocities of $H_2/O_2/N_2$ mixtures at 0.35–4.00 atm and 298 K with volumetric N_2 concentrations of 79.0–87.5% within the oxidizer. Kwon and Faeth [24] studied freely (outwardly) propagating spherical laminar premixed H_2/O_2 flames to observe the dilution effect of He, Ar, and N_2 on the S_u^o at 0.3–3.0 atm and 298 K, with volumetric oxygen concentrations in the nonfuel gases of 21%–36%. Lamoureux et al. [25] presented experimental flame speed data for H_2/air mixtures diluted with mixtures containing up to 40% He and carbon dioxide (CO_2) at 1 bar and 298 K. Qiao et al. [26] investigated the suppression effects of He, Ar, N_2, and CO_2 diluents on laminar premixed H_2/air flames at 0.5–1.0 atm, 300 K, and 0–40% dilution ratios.

Hu et al. [27] utilized the constant pressure method for spherically expanding H_2/air flames diluted with N_2, CO_2, and a mixture of 15% CO_2 + 85% N_2 at 1 bar, 303 K, and dilution ratios of 0–15% in order to obtain the S_u^o and L_b. Hermanns et al. [28] measured adiabatic burning velocities for $H_2/O_2/N_2$ mixtures at 1 bar and 298 K with oxygen content of 7–10% in the oxidizer using a heat flux burner. At 1 bar and 350–600 K, Paidi et al. [29] experimentally analyzed the S_u^o of H_2/air mixtures diluted with N_2 or CO_2 with 60–80% diluent concentration in the fuel. Santner et al. [30] examined the kinetic effects of water vapor addition on the burning rates of H_2/O_2/He mixtures at 1–10 atm and flame temperatures between 1600 K and 1800 K. Li et al. [31] determined laminar combustion characteristics of H_2/air mixtures diluted with N_2 or CO_2 from spherically expanding flames at 1 bar and 298 K for 0–60% diluent levels within the fuel.

In an optically accessible constant volume combustion chamber, Yang et al. [32] measured the S_u^o for H_2/O_2 mixtures diluted with He and CO_2 at 0.25–20 atm of initial pressures, 1300–2200 K of flame temperatures, and 15–75% of diluent concentrations within the reactants. Lyu et al. [33] studied Bunsen burner H_2/air flames with steam dilution (up to 33% by volume) at 1–5 atm and 373–440 K. Using spherically expanding flame approach, Lu et al. [34] obtained the S_u^o of H_2/O_2 flames with various diluents, namely He, Ar, N_2, and CO_2, at 1–4 bar, 298 K, and 80.0–90.9% dilution within the oxidizer. To the best of the authors' knowledge, the only experimental H_2 laminar flame speed study investigating the dilution effect of actual main residuals of H_2/air combustion (N_2 + H_2O) was conducted by Duan and Liu [35] at 1 bar, 393 K, and 0–40% dilution ratios.

As summarized above, in spite of the abundance of experimental studies on the S_u^o and L_b of diluted H_2/oxidizer mixtures, studies investigating the dilution effect of actual main combustion residuals of H_2/air mixtures (N_2 + H_2O) are very scarce. However, Duva et al. [36] and Galmiche et al. [37] demonstrated that combustion products used as a diluent

cannot be interchanged with different exhaust and/or inert gases as each flue gas has distinct thermodynamic, transport, and chemical properties, which also vary substantially with pressure and temperature. For instance, CO_2 and H_2O are chemically more active than He, Ar, and N_2 since CO_2 and H_2O actively participate in elementary chemical reactions and have higher relative third-body efficiencies [36]. CO_2 also causes the largest reduction in the S_u^o and the greatest change in the flame stability with its higher specific heat capacity and lower thermal diffusivity [36]. As a result, critical errors may occur in the S_u^o and L_b due to the replication of actual main combustion residuals with different exhaust and/or inert gases.

The present study examines the dilution effect of actual main residuals of H_2/air combustion on the S_u^o and L_b of H_2/air mixtures at 1 and 2 bar, 373, 423, and 473 K, and equivalence ratio (φ) of 0.7. The φ is selected as 0.7 because the equivalence ratio of lean burn combustion within a gas turbine is typically around 0.3–1.0 [11,38–41] and the preferential cellular formation on the H_2 flame surface is suppressed with increasing φ, which enables the laminar flame speed measurements. Due to concerns about the diluents listed above, a mixture of 65% N_2 + 35% H_2O by mole, which represents the primary components of H_2/air combustion residuals, is used for dilution. 0–50% diluent levels are tested experimentally and numerically with 10% increments, but the results at the 50% diluent level are not presented due to the buoyant instability on the flame front. The dilution ratio is defined as the percentile concentration of the diluent within the reactants. Experimental results are compared with numerical data obtained by several chemical mechanisms in order to assess the accuracy of these mechanisms. Numerical findings and sensitivity analyses are used to investigate impacts of the diluent on the S_u^o, adiabatic flame temperature (T_{adb}), and flame stability.

Specifications of experimental approach and simulation model

Experimental methodology

In the present study, the S_u^o and L_b values are deduced from spherically expanding H_2/air/diluent flames in an optically accessible constant volume combustion chamber. The details of the experimental set-up are discussed extensively in the authors' previous publications [42,43] and the combustion chamber has been validated with methane/air flames at 1 bar and 298 K [44], propane/air flames at 1 bar and 298 K [45], and iso-octane/air flames at 1 bar and 373 K [46]. Thus, the experimental apparatus is only briefly mentioned here.

Initial combustible mixtures are prepared inside the 22.24-L preheated cylindrical combustion vessel starting with the reactant which has the smallest concentration. Post combustion gases are evacuated with a vacuum pump after each test, then the chamber is purged with air and the system is vacuumed again before starting a new test. H_2, air, and N_2 are supplied to the system with a heated gas manifold which is connected to the main body of the chamber with a high pressure shutoff and regulating valve. H_2O is directly injected into the vessel with a high pressure fuel injection system. The φ and dilution ratio are adjusted with the ideal gas law and partial pressures of the reactants which are measured with an absolute pressure transducer on the heated gas manifold. Maximum deviation in the φ from the desired value of 0.7 is 0.0028 while the highest random uncertainty in the dilution ratio is 0.13%. Before firing, the reactants are mixed with a stirrer, which is turned off prior to ignition.

The constant pressure method is employed for flame speed calculations and, therefore, measurements are limited to the early stage of combustion where the pressure is constant. According to this method, the flame speed of the stretched burned gases (S_b) is equal to the time derivative of the cold spherical flame front radius (R_f), i.e. $S_b = dR_f/dt$. The R_f is calculated with an in-house image processing code [47] from schlieren images, which are recorded with a z-type schlieren set-up [48] at 12,000 Hz after the initiation of the combustion in the middle of the vessel with an inductive ignition system. Then, a third-order polynomial is fitted to the radius-time history and differentiated to obtain the S_b.

The linear stretch model between the flame curvature and the flame speed, i.e. Eq. (1), which was first proposed by Markstein [49] and recently revisited by Chen [50], and the nonlinear stretch model of Kelley and Law [51], i.e. Eq. (2), which was obtained from the asymptotic analysis of Ronney and Sivashinsky [52] for adiabatic spherical flames, are used to calculate the flame speed of the unstretched burned gases (S_b^o) and L_b. With detailed numerical simulations and theoretical analysis, it was shown that Eq. (1) better represents the actual behaviour between the flame speed and flame stretch for mixtures with a positive L_b whereas Eq. (2) is more appropriate for mixtures with a negative L_b [50,53,54]. Therefore, depending on the L_b of the tested mixture, Eq. (1) or Eq. (2) is least-squares fitted to the experimental data on the plot of S_b vs. $^2/_{R_f}$ for Eq. (1) and on the plot of $\ln(S_b)$ vs. $^2/_{(S_b R_f)}$ for Eq. (2) and extrapolated to $\lim_{R_f \to \infty}\left(\frac{2}{R_f}\right)$ for Eq. (1) and to $\lim_{R_f \to \infty}\left[{}^2/_{(S_b R_f)}\right]$ for Eq. (2), as shown in Fig. 1. While the slopes of these plots provide $(-S_b^o L_b)$, the y-intercept of $\ln(S_b)$ vs. $^2/_{(S_b R_f)}$ equals $\ln(S_b^o)$ and the y-intercept of S_b vs. $^2/_{R_f}$ is S_b^o. Lastly, the S_u^o, which is also called the laminar flame speed, is calculated from the mass flow balance at an infinitely thin flame front, i.e. Eq. (3), in which ρ_b and ρ_u correspond to burned and unburned gas densities and are computed with numerical simulations.

$$S_b = S_b^o - S_b^o L_b \frac{2}{R_f} \tag{1}$$

$$\frac{S_b}{S_b^o}\ln\left(\frac{S_b}{S_b^o}\right) = -\frac{2L_b}{R_f} \tag{2}$$

$$S_u^o = \frac{\rho_b}{\rho_u} S_b^o \tag{3}$$

Since the S_u^o values reported in the present study are greater than or equal to 26 cm/s, the reduction in the S_u^o due to the radiation induced cooling effect is estimated as less than 2% [55]. To minimize radiation and confinement induced flow

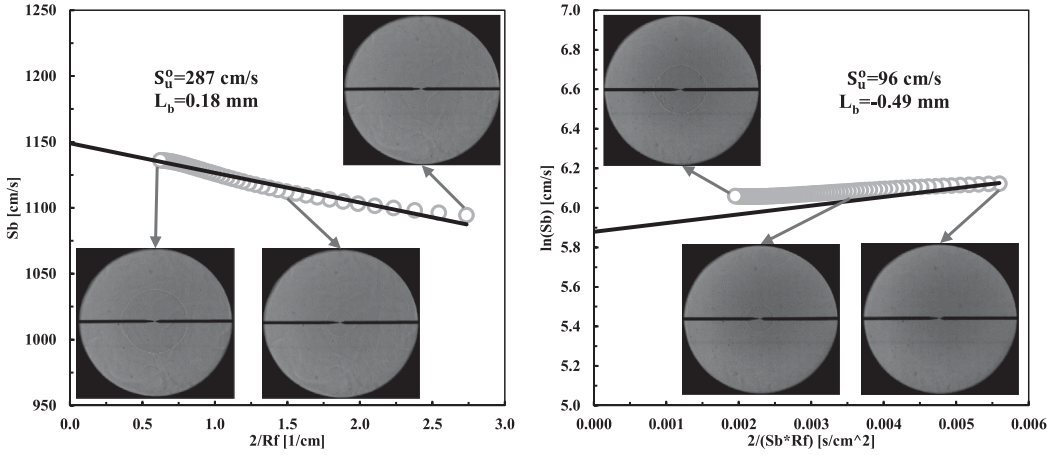

Fig. 1 – Extrapolation of stretch models - Eqs. (1) and (2) - for H_2/air flames at 1 bar, 473 K, 0% diluent level, and $\varphi = 0.7$ (Left) and 1 bar, 373 K, 20% diluent level, and $\varphi = 0.7$ (Right).

effects, the S_u^o calculations are limited to the schlieren images where the total spherical flame volume is smaller than 25% of the vessel inner volume, which suggests that the reduction in S_u^o due to radiation and confinement induced flow effects is within 2–3% [56,57]. Nevertheless, whenever preferential and/or hydrodynamic cellularity is detected prior to the upper measurement limit, the S_u^o calculations are stopped with the commencement of cellular formation. In order to prevent the S_u^o calculations from being affected by the spark/ignition energy during the propagation of the early flame kernel, H_2/air/diluent mixtures at the desired test points are ignited with different discharge energies close to the minimum ignition energy of the mixture at that particular initial condition. Subsequently, all experimental results at the same test point are plotted on the R_f versus S_b graph and the S_u^o calculations are started at the R_f, where the S_b curves from all experiments at the same test point first converge.

Numerical methods

Chemical kinetic simulations are performed using the H_2 chemical mechanisms of NUI Galway-H_2 [58], San Diego [59], HP-Mech [60], Princeton-H_2 [61], Vrije-H_2 [62], and USC-H_2 [63] incorporated into CHEMKIN-PRO [64]. To model the flame speed measurements, a premixed laminar flame simulator with an external inlet gas source and an outlet flow from the reactor is used together with specifications of the initial conditions (temperature, pressure, equivalence ratio, diluent level etc.) and the thermodynamic and transport properties of the species. The first solution is attained for a large computational region with a fixed flame coordinate system so that the computational domain is unconstrained by the boundaries and the mass and heat diffusions can be neglected. Afterwards, mesh independency is achieved by increasing the number of grid points and refining the adaptive grid controls.

The NUI Galway-H_2 chemical mechanism [58], comprising of 21 reactions and 10 species, was developed to simulate H_2/O_2 flame structure and propagation, and ignition phenomena at 298–2700 K, 0.05–87 atm, and $\varphi = 0.2$–6.0. It is based on the kinetic mechanism of Mueller et al. [65] and has good overall performance in predicting ignition delay time and laminar flame speed of H_2/oxidizer mixtures [66,67]. The San Diego kinetic scheme [59] consists of 311 reactions and 68 species with sub-mechanism for N_2 chemistry and is capable of the reproduction of H_2 flame velocity measurements especially at high temperatures [66,67]. The HP-Mech [60], comprising of 615 reactions and 89 species, is a high pressure mechanism for H_2, CO, CH_2O, CH_4, CH_3OH, C_2H_2, C_2H_4, and C_2H_6 with a particular focus on CO_2 and H_2O dilution effects and has been tested against various validation targets for diluted H_2 flames [68].

The Princeton-H_2 kinetic model [61], comprising of 25 reactions and 13 species, is also based on the chemical mechanism of Mueller et al. [65] and validated against a wide range of experimental conditions (298–3000 K, 0.3–87 atm, and $\varphi = 0.25$–5.0) for H_2/O_2 mixtures. The Vrije-H_2 kinetic mechanism [62], comprising of 75 reactions and 15 species, was developed for H_2 combustion and has good overall performance in predicting ignition delay time and laminar flame speed of H_2/oxidizer/diluent mixtures especially at low temperatures [66,67]. The USC-H_2 [63] mechanism, comprising of 38 reactions and 14 species, is a chemical model for high temperature H_2 and CO oxidation, which was developed by optimizing the H_2/CO sub-mechanism of GRI-Mech 3.0 [69] against various H_2-CO combustion data (shock tube ignition delay time, laminar flame speed, and extinction strain rate). The model has good agreement with experimental data at low temperatures [66]. For clarity, all H_2 chemical mechanisms explained above are summarized in Table 1.

An analysis of sensitivity coefficients with respect to the S_u^o is carried out in order to identify the essential reactions for the flame speed prediction. The first-order sensitivity coefficient of the flow rate to the pre-exponential A-factor in the Arrhenius reaction-rate expressions of each reaction rate coefficient is computed and normalized in the CHEMKIN-PRO [64]. The

Table 1 – Overview of the chemical kinetic mechanisms considered in the present study.

	NUI Galway-H_2 [58]	San Diego [59]	HP-Mech [60]	Princeton-H_2 [61]	Vrije-H_2 [62]	USC-H_2 [63]
Number of species	10	68	89	13	15	14
Number of reactions	21	311	615	25	75	38

positive sensitivity coefficient value indicates that the reaction increases the S_u^o [70,71].

Results and discussion

This section begins with the validation of the present experimental approach with non-diluted H_2/air mixtures at 1 bar and 298 K. Subsequently, effects of pressure, temperature, and dilution ratio changes on the S_u^o and L_b of H_2/air flames are examined with measurement results at 1–2 bar, 373–473 K, 0–40% dilution ratios, and $\varphi = 0.7$. At least three successful experiments were performed for each test point. The standard deviation of the measurement results at the same test point is specified as the overall uncertainty in the S_u^o and L_b and shown as error bars in the following figures.

Numerical S_u^o data obtained by several chemical mechanisms are compared against experimental findings to evaluate their accuracy in predicting the S_u^o for diluted H_2/air mixtures. The kinetic model, which had the best agreement with the present measurement results, is then used for a series of additional numerical simulations, sensitivity analysis, and T_{adb} calculations in order to quantify the impacts of the diluent on the S_u^o. All experimental and numerical results with their corresponding uncertainties are provided in the supplementary material.

Validation of the experimental method

Due to the abundance of experimental H_2 flame speed results at/around standard ambient temperature and pressure, the S_u^o of non-diluted H_2/air mixtures at 1 bar, 298 K, and $\varphi = 0.7–4.0$ is chosen as a validation target. Four experimental S_u^o data sets obtained by different research groups after 2010, namely State Key Laboratory of Multiphase Flow in Power Engineering at Xi'an Jiaotong University, Institute for Energy and Nuclear Energy at Karlsruhe Institute of Technology, Peterson Research Group at Texas A&M University, and Institute for Combustion Technology at RWTH Aachen University, are used for comparison to the present measurements. Experimental results at $\varphi = 0.7$, 0.8, 1.3, 2.0, 3.5, and 4.0, which are presented in one of the authors' previous publication [45], are utilized for the validation of the experimental method. In addition to these results, extra measurements are performed at $\varphi = 0.9$, 1.0, 1.1, 1.7, 2.2, 2.4, 2.6, and 3.0 in the current study.

S_u^o values of H_2/air mixtures at 1 bar and 298 K from the present study are plotted against experimental results of Dong et al. [72], Kuznetsov et al. [73], Krejci et al. [74], and Beeckmann and Pitsch [75] in Fig. 2. Similar to the current work, Kuznetsov et al. [73], Krejci et al. [74], and Beeckmann and Pitsch [75] deduced the S_u^o from spherically expanding flames at constant pressure whereas Dong et al. [72] used a Bunsen burner to measure hydrogen flame speeds. The present S_u^o data show good agreement with the burner results of Dong et al. [72] at $\varphi < 1.7$. At higher equivalence ratios, Dong et al. [72] provided slightly faster flame speeds (up to 4%) than the current findings. Kuznetsov et al. [73] measured considerably slower flame speeds than other researchers in Fig. 2 at $\varphi < 1.3$ and their flame speeds are somewhat faster than the ones obtained by the current authors and Krejci et al. [74] at higher equivalence ratios.

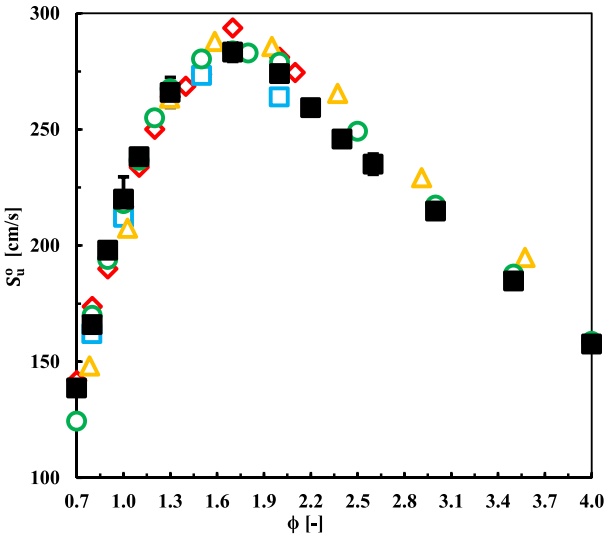

Fig. 2 – Comparison of present S_u^o data for H_2/air mixtures at 1 bar and 298 K with previously published experimental results (black squares – current findings, red diamonds - Dong et al. [72], orange triangles - Kuznetsov et al. [73], green circles - Krejci et al. [74], and blue squares - Beeckmann and Pitsch [75]). (For interpretation of the references to colour in this figure legend, the reader is referred to the Web version of this article.)

Excellent agreement is observed between the present S_u^o data for H_2/air mixtures at 1 bar and 298 K and results of Krejci et al. [74] except at $\varphi = 0.7$. The S_u^o value of Krejci et al. [74] at $\varphi = 0.7$ is significantly slower than other results in Fig. 2. The findings of Beeckmann and Pitsch [75] are very similar to other flame speed results in Fig. 2 for $\varphi \leq 1.5$. At $\varphi = 2.0$, Beeckmann and Pitsch [75] measured slightly slower flame speed compared to Dong et al. [72], Kuznetsov et al. [73], Krejci et al. [74], and the current work. In brief, results presented in Fig. 2 are generally consistent with each other although previously published S_u^o data are slightly dispersed.

Experimental S_u^o data

As shown in Fig. 3, the S_u^o increases from 186 cm/s to 228 cm/s and from 228 cm/s to 287 cm/s with an initial temperature

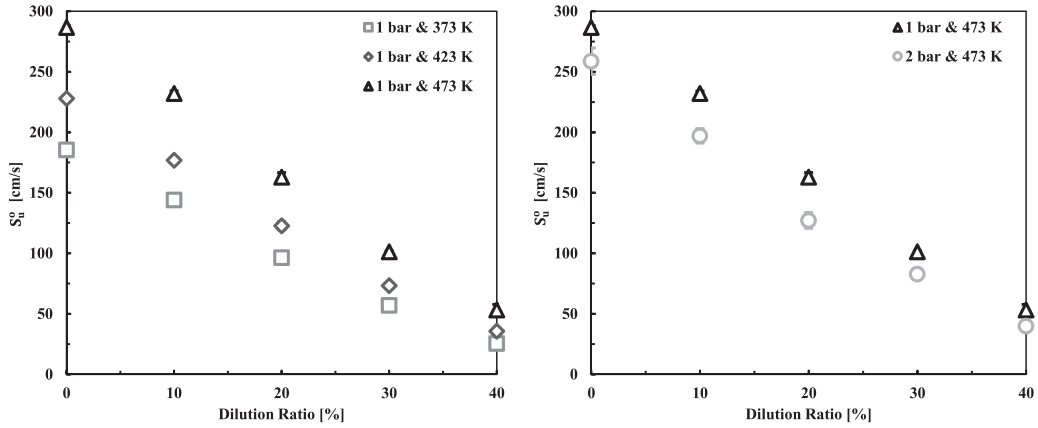

Fig. 3 – Experimental S_u^o results at 1 bar, 373–473 K, 0–40% diluent levels, and φ = 0.7 (Left) and 1–2 bar, 473 K, 0–40% diluent levels, and φ = 0.7 (Right).

change from 373 K to 423 K and from 423 K to 473 K, respectively, for non-diluted H_2/air mixtures at 1 bar primarily because of boosted dissociation reactions and greater burned to unburned gas density ratios [76]. The increase in the S_u^o because of the initial temperature variation from 423 K to 473 K is larger than the one from 373 K to 423 K, which also holds true for all dilution ratios (0–40%), though increases in the T_{adb} for both unburned gas temperature rises are almost identical (37–42 K) and the expansion ratio increases more between 373 K and 423 K. This suggests that enhanced dissociation reaction rates have a greater importance in the S_u^o increase due to increased unburned gas temperature. Although increases in the T_{adb} due to the initial temperature rise are similar for all diluent levels, the increase in the S_u^o with the unburned gas temperature gets smaller at high dilution ratios. However, the percentile changes in the S_u^o because of the initial temperature rise are still greater at higher diluent levels.

The initial pressure change from 1 bar to 2 bar at 473 K decreases the S_u^o from 287 cm/s to 259 cm/s, from 232 cm/s to 197 cm/s, from 163 cm/s to 127 cm/s, from 101 cm/s to 83 cm/s, and from 53 cm/s to 40 cm/s at 0%, 10%, 20%, 30%, and 40% dilution ratios, respectively, primarily because of deteriorated dissociation reactions and reduced active radicals [76]. At elevated pressures, H radical consumption of $H + O_2 + M \leftrightarrow HO_2 + M$ increases, diminished H radicals inhibit $H + O_2 \leftrightarrow O + OH$, and therefore the flame speed decreases [76]. On the other hand, the T_{adb} values of H_2/air mixtures at 1 and 2 bar are almost identical.

As shown in Fig. 3, the addition of the dilution mixture (a mixture of 65% N_2 + 35% H_2O by mole) to H_2/air mixtures at 1–2 bar and 373–473 K lowers the S_u^o almost linearly (especially for the diluent levels less than 40%) primarily because of the reduced H_2/air concentration and active radicals. The slopes of these imaginary descending flame speed vs. dilution ratio lines increase with increasing temperature because more pronounced decreases in the S_u^o are observed at elevated temperatures with increasing diluent level. The nearly linear correlation between the S_u^o and dilution ratio is attributable to the high concentration of chemically almost inactive N_2 within the dilution mixture. However, there is still a fair amount of H_2O in the dilution mixture with a generally high third-body collision efficiency, which prevents the relation between the S_u^o and dilution ratio from being thoroughly linear.

An empirical flame speed correlation in the form of Metghalchi and Keck's power law [77] is fitted to the present experimental S_u^o results. A linear expression is used in the nonlinear regression model for the dilution effect on the S_u^o. The model coefficients are optimized with the generalized reduced gradient method [78] in order to minimize the standard deviation of discrepancies between experimental findings and correlation predictions, i.e. the root mean square error (RMSE). As a result of the nonlinear optimization of the correlation coefficients, a completely empirical S_u^o correlation with an RMSE of 6.78 cm/s is developed as Eq. (4) where T is the unburned gas temperature in K, P is the pressure in bar, and X is the dimensionless dilution ratio (e.g. 0.30 - not 30%). Note that higher degrees of polynomials are

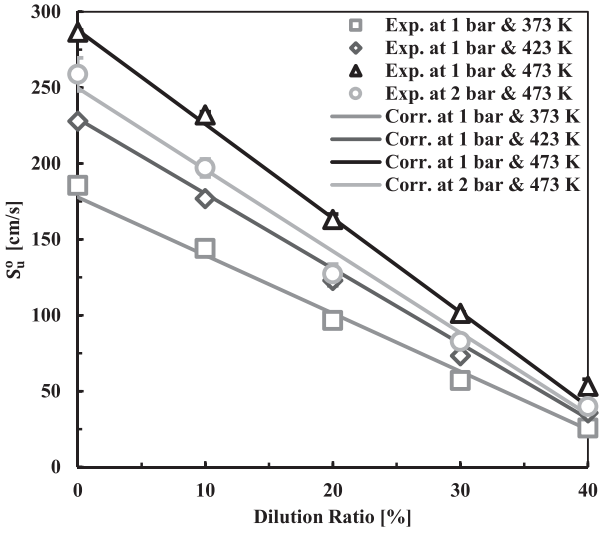

Fig. 4 – Comparison of correlation predictions with measured S_u^o data at 1–2 bar, 373–473 K, 0–40% diluent levels, and φ = 0.7.

also examined for the dilution effect, but a noteworthy enhancement in the correlation results is not observed. Lastly, the S_u^o predictions of Eq. (4) are compared against the current experimental data in Fig. 4.

$$S_u^o = 186 * \left(\frac{T}{298}\right)^{2.030} * \left(\frac{P}{1}\right)^{-0.205} * (0.606 - 1.305 * X) \quad (4)$$

Experimental L_b data

Hydrodynamic (Darrieus-Landau) and thermal diffusive (preferential-diffusion) effects are crucial for lean laminar hydrogen flame stability. These effects wrinkle the smooth spherical flame front and induce cellularity due to a small flow perturbation, such as a solid body, pressure pulses, or acoustic oscillations [79], and therefore, increase the flame surface area and the flame propagation speed [80]. The hydrodynamic cellularity arises from wrinkles on the flame surface which is a result of small hydrodynamic flow disturbances [81]. The hydrodynamic cellularity is governed by the flame thickness and expansion ratio. The preferential cellularity is a result of the preferential diffusion of mass compared to heat within the flame, which causes a change in local equivalence ratio and flame speed, and is observable when the mass diffusivity of the deficient reactant is adequately greater than the thermal diffusivity of the mixture [82]. The preferential cellularity is governed by Lewis number and therefore L_b.

Fig. 5 illustrates the L_b variation with unburned gas temperature, initial pressure, and dilution ratio changes. The L_b values of H_2/air mixtures in Fig. 5 are negative except for very low diluent levels (≤10%) at 1 bar. This suggests that the preferential cellular formation is inevitable for the majority of test points. In other words, the lean H_2/air flames tested in the present study are mostly subject to the thermal diffusive instabilities. At low dilution ratios (≤20%), there is little influence of temperature on L_b, which was also observed by Duva et al. [83] for slightly diluted methane/air flames (≤15%). However, at higher diluent levels (>20%), the L_b increases with increasing initial temperature, which implies that highly diluted lean H_2/air flames at lower temperatures are more stretched than the ones at elevated temperatures. Moreover, intensified reaction rates at high temperatures lessen the laminar flame thickness, which promotes the Darrieus-Landau instabilities.

Fig. 5 demonstrates that lean H_2/air flames at 2 bar and 473 K are thermal diffusively less stable than the ones at 1 bar and 473 K for low dilution ratios (≤20%). However, at higher diluent levels (≥30%), the initial pressure effect on the L_b is generally inappreciable. Additionally, an increase in the combustion pressure leads to thinner H_2 laminar flame thickness and therefore results in earlier inception of hydrodynamic cellular formation on the flame surface.

The L_b values of H_2/air mixtures generally decrease with increasing dilution ratio. Addition of dilution mixture into the

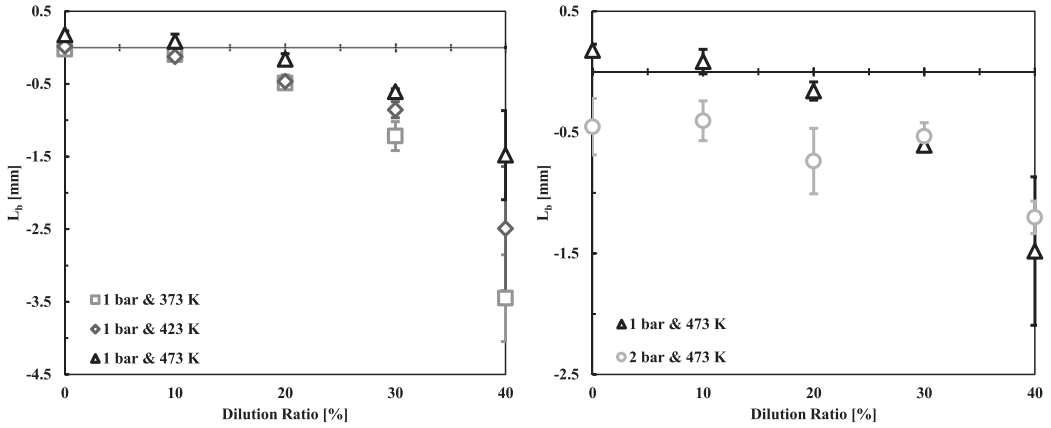

Fig. 5 – Experimental L_b results at 1 bar, 373–473 K, 0–40% diluent levels, and φ = 0.7 (Left) and 1–2 bar, 473 K, 0–40% diluent levels, and φ = 0.7 (Right).

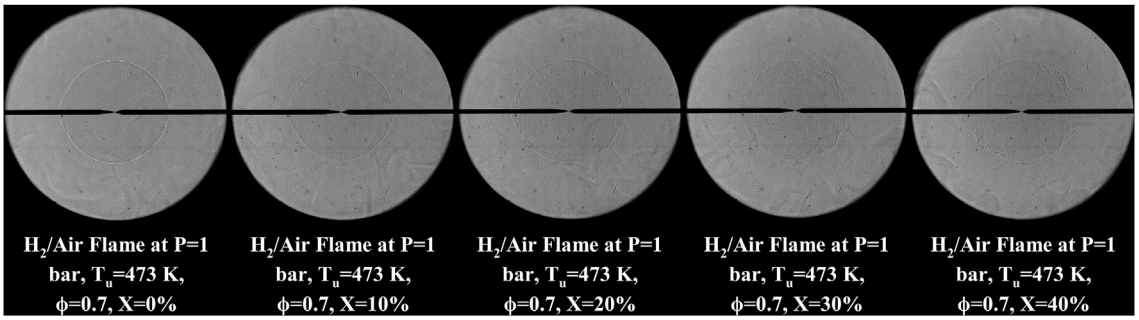

Fig. 6 – Schlieren images showing the flame front instabilities.

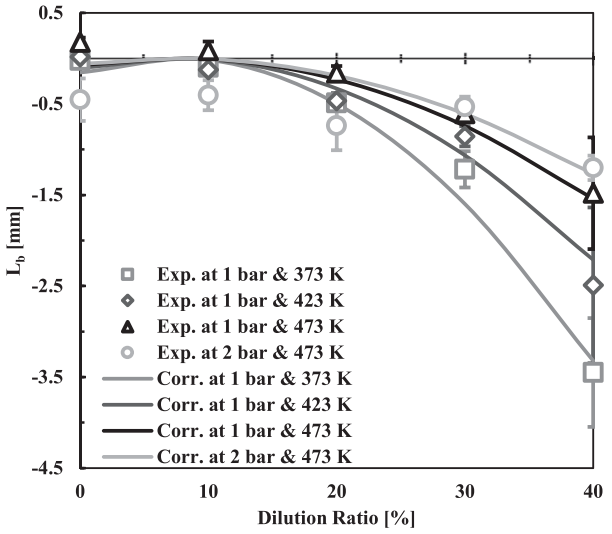

Fig. 7 – Comparison of correlation predictions with measured L_b data at 1–2 bar, 373–473 K, 0–40% diluent levels, and $\varphi = 0.7$.

reactants alters the thermal/heat and mass diffusivities of the initial air/fuel mixture. Consequently, the Lewis number of the combustible mixture decreases, which makes the highly diluted H_2/air flames more stretched. On the contrary to the change in the S_u^o, the L_b decline due to the increasing dilution ratio is not linear. Generally, larger decreases are observed in the L_b with high diluent levels because the dilution mixture has greater influence on the mixture Lewis number at high dilution ratios due to its larger concentration within the reactants. Furthermore, addition of the dilution mixture to the reactants increases the H_2 laminar flame thickness and therefore lowers the Darrieus-Landau instability effects. Fig. 6 depicts the H_2 flame stability change with diluent addition.

Similar to the data fitting that is discussed previously for the experimental S_u^o data, an empirical burned gas Markstein length correlation in the form of Metghalchi and Keck's power law [77] is adopted for the present experimental L_b results. A quadratic expression is utilized in the nonlinear regression model for the dilution effect on the L_b. Higher degrees of polynomials are also examined for the dilution effect, but a noteworthy enhancement in the correlation results is not observed. The model coefficients are optimized with the

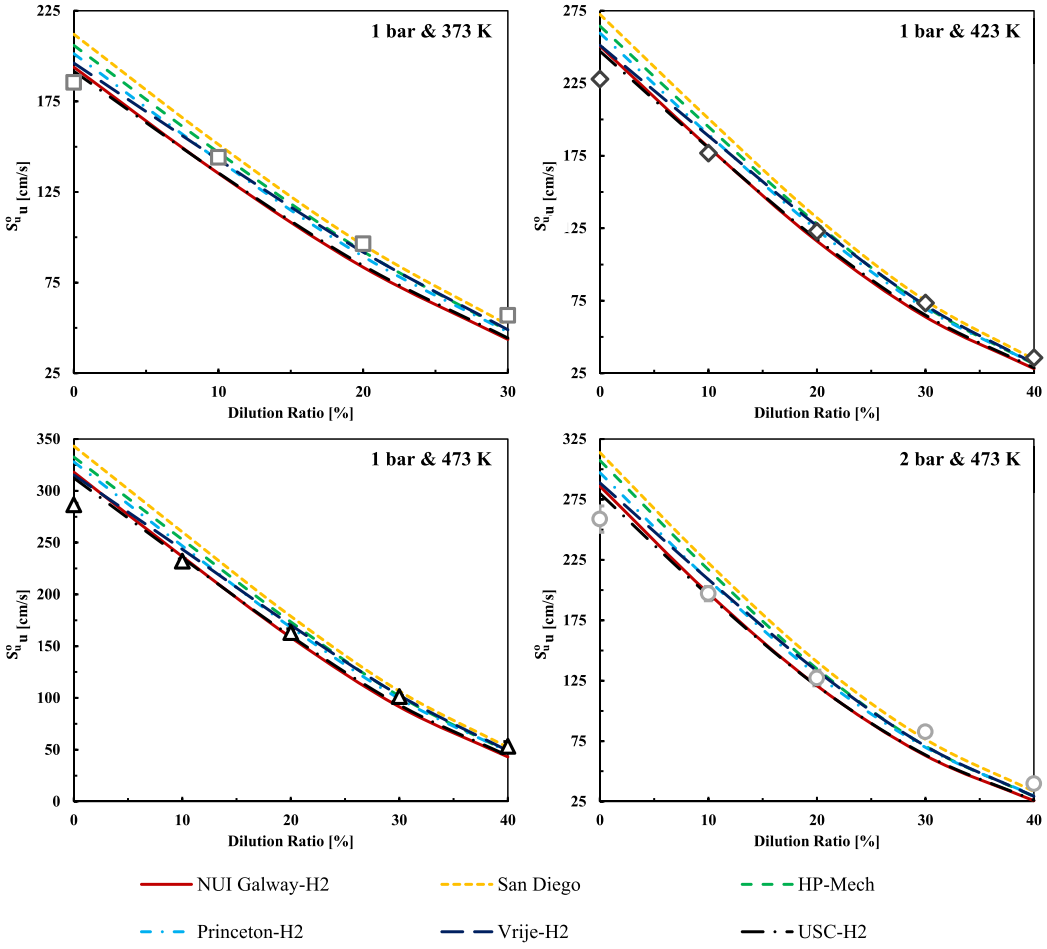

Fig. 8 – Comparison of numerical S_u^o predictions with experimental measurement results at 1–2 bar, 373–473 K, 0–40% diluent levels, and $\varphi = 0.7$ (markers - experimental data and lines - numerical data).

generalized reduced gradient method [78] in order to minimize the standard deviation of discrepancies between the experimental findings and the correlation predictions, i.e. the root mean square error (RMSE). As a result of the nonlinear optimization of the correlation coefficients, a completely empirical L_b correlation with an RMSE of 0.24 mm is developed as Eq. (5) where T is the unburned gas temperature in K, P is the pressure in bar, and X is the dimensionless dilution ratio (e.g. 0.30 - not 30%). Lastly, the L_b predictions of Eq. (5) are compared against the current experimental data in Fig. 7.

$$L_b = \left(\frac{T}{298}\right)^{-3.231} * \left(\frac{P}{1}\right)^{-0.283} * \left(-0.319 + 9.271 * X - 64.052 * X^2\right) \quad (5)$$

Chemical kinetic analysis

Detailed chemical mechanisms for H_2 combustion are vital for chemical kinetic analysis since they serve as the core of any detailed hydrocarbon kinetic model. Gas turbine engine manufacturers mainly rely on numerical analysis (computational fluid dynamics) in the early design stage where experiments are rather costly [66]. Accuracy of numerical predictions for H_2 combustion (and for any hydrocarbon combustion in general) depends on high precision in H_2 chemical mechanisms, which should be verified/optimized against experimental data for H_2/oxidizer mixtures. Therefore, the chemical kinetic simulations in this study are performed by incorporating several H_2 chemical mechanisms in CHEMKIN-PRO [64], namely NUI Galway-H_2 [58], San Diego [59], HP-Mech [60], Princeton-H_2 [61], Vrije-H_2 [62], and USC-H_2 [63]. The numerical S_u^o results are then compared with experimental findings to assess the accuracy of the mechanisms.

The results of the numerical and experimental data comparison are illustrated in Fig. 8 and summarized in Table 2. Note that the numerical S_u^o values can be successfully calculated up to a 30% dilution ratio at 1 bar and 373 K. Therefore, measurements at 1 bar, 373 K, and 40% diluent level are not included in Fig. 8. The RMSE values in Table 2 correspond to standard deviations of differences between experimental S_u^o findings and numerical S_u^o predictions. All investigated chemical mechanisms capture the general/overall trend of the experimental results adequately, but they over-predict flame speeds for non-diluted H_2/air mixtures (by up to 21%), which occurs more profoundly at higher pressures and temperatures. These over-predictions are greater for the San Diego [59] and HP-Mech [60] kinetic models. On the other hand, the NUI Galway-H_2 [58] and USC-H_2 [63] provide the closest S_u^o to experimental findings at low dilution ratios (≤20%).

The accuracies of the tested chemical mechanisms are generally superior at 20–30% dilution ratios. At higher diluent levels (≥30%), they slightly underestimate flame speed, but their predictions are still more consistent with the experimental results than they are at low dilution ratios (≤10%). As shown in Fig. 8, these underestimations are larger at higher pressures and lower temperatures. The NUI Galway-H_2 [58] and USC-H_2 [63] models predict very similar S_u^o data, but the USC-H_2 [63] is slightly more accurate than the NUI Galway-H_2 [58]. In fact, among the tested kinetic mechanisms, the USC-H_2 [63] shows the best agreement with experimental results whereas the San Diego [59] has the poorest agreement with measurements. The Princeton-H_2 [61] and Vrije-H_2 [62] also predict almost identical S_u^o values, which are more consistent with experimental data at high dilution ratios (≥20%).

Diluent impacts

There are three primary impacts of the dilution mixture on the S_u^o of H_2/air flames, namely the dilution effect, thermal-diffusion effect, and chemical/kinetic effect [84]. The addition of a mixture of 65% N_2 + 35% H_2O by mole to the reactants decreases the non-inert gas concentration within the combustible mixture, which yields a decreased net reaction rate, T_{adb}, and S_u^o. This phenomenon is called the dilution effect [85]. The dilution mixture also alters the thermodynamic and transport properties of the reactants, which initially (before dilution) consist only of H_2 and air. This alteration is known as the thermal-diffusion effect [84] and has an influence on both flame speed and stability. For example, the unburned gas density, mixture specific heat capacity, and

Table 2 – Summary of the numerical and experimental S_u^o data comparison.

Mechanism	RMSE	Comments
NUI Galway-H_2 [58]	14 cm/s	• Closest S_u^o to experimental findings at low dilution ratios • Slightly poorer accuracy than San Diego [59], HP-Mech [60], Princeton-H_2 [61], and Vrije-H_2 [62] at high dilution ratios (≥30%)
San Diego [59]	20 cm/s	• Poorest agreement with experimental results • Large over-prediction for non-diluted mixtures • Consistently increasing accuracy with increasing dilution ratios
HP-Mech [60]	18 cm/s	• Large over-prediction for non-diluted mixtures • Generally increasing accuracy with increasing dilution ratios
Princeton-H_2 [61]	16 cm/s	• Very similar S_u^o predictions with Vrije-H_2 [62] • Generally increasing accuracy with increasing dilution ratios
Vrije-H_2 [62]	15 cm/s	• Very similar S_u^o predictions with Princeton-H_2 [61] • Generally increasing accuracy with increasing dilution ratios
USC-H_2 [63]	12 cm/s	• Best agreement with experimental results • Closest S_u^o to experimental findings at low dilution ratios • Slightly poorer accuracy than San Diego [59], HP-Mech [60], Princeton-H_2 [61], and Vrije-H_2 [62] at high dilution ratios (≥30%)

thermal and mass diffusivities are changed due to the thermal-diffusion effect of the dilution mixture, which results in a variation in the S_u^o, L_b, and T_{adb}. Lastly, the components of the dilution mixture participate in elementary kinetic reactions and lower the S_u^o and T_{adb} by varying reaction kinetics, i.e. the chemical effect [84]. Two factors are primarily responsible for the chemical effect, (1) the direct participation of the dilution mixture components in elementary reactions and (2) the participation of the dilution mixture components in third-body reactions.

In order to determine the strength of these two chemical effect factors separately, two additional sets of CHEMKIN-PRO [64] flame speed simulations are performed in addition to the original chemical kinetic analyses presented in the previous section (first set of numerical data). The USC-H_2 chemical mechanism [63] is used for the additional analyses since it shows the best agreement with experimental results. Initially, the flame speed simulations are repeated with the H_2/air mixtures (this time) diluted with chemically inactive N_2 and H_2O, which have the same third-body collision efficiencies as the original N_2 and H_2O and are added to the chemical mechanism and transport and thermodynamic data files. Therefore, this second set of numerical data contains all of the impacts of the dilution mixture except the chemical effect due to the direct participation of the dilution mixture components in elementary reactions. Similarly, the third set of numerical data is deduced from flame speed simulations of H_2/air mixtures (again) diluted with chemically inactive N_2 and H_2O, which (this time) have zero third-body collision efficiencies. As a result, this third set of numerical data does not include the chemical effects of the dilution mixture at all. A comparison of the flame speed results from these three numerical data sets enables the determination of the separate impacts of the two chemical effect factors on the S_u^o, with results shown in Fig. 9.

As can be seen in Fig. 9, for the initial conditions tested in the present work, the dilution and thermal-diffusion effects (combined) are primarily responsible for the decrease in the S_u^o with the diluent addition. At 1 bar, the total contribution of the dilution and thermal-diffusion effects on the reduction in the S_u^o ranges from 87% to 91%. In other words, the combined effect of dilution and thermal-diffusion is not significantly affected by the temperature and dilution ratio changes. The remaining reduction in the S_u^o can be attributed to the chemical effect, the majority of which comes from the participation of the dilution mixture components in third-body reactions. The chemical effect due to the direct participation of the dilution mixture components in elementary reactions has a very minor impact on the decrease in the S_u^o and it gets even less notable at higher dilution ratios due to the decreased T_{adb} at these conditions.

At 2 bar, the dilution and thermal-diffusion effects (combined) drop to 83–91%, while the contribution of the chemical effect due to the participation of the dilution mixture components in third-body reactions increases by up to 13%. The reason behind this change is that the H radical consumption

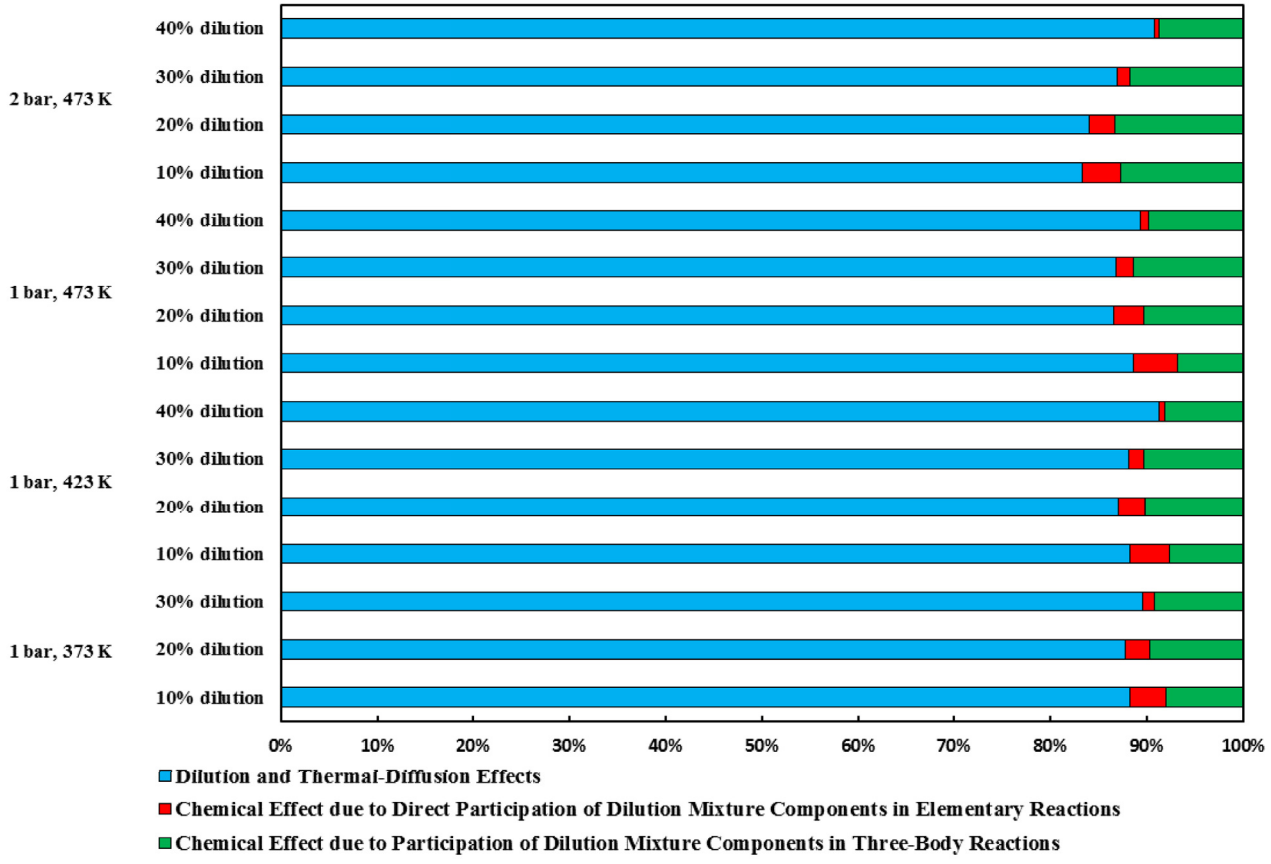

Fig. 9 – Breakdown of the dilution mixture effects on the S_u^o.

from the $H + O_2 + M \leftrightarrow HO_2 + M$ reaction accelerates at elevated pressures, which reduces the H radical pool and therefore inhibits the $H + O_2 \leftrightarrow O + OH$ reaction [76]. The overall characteristics of the chemical effect due to the direct participation of the dilution mixture components in elementary reactions are unchanged from 1 bar to 2 bar.

In the Experimental S_u^o Data section, it is shown that there is almost a linear relation between the S_u^o and dilution ratio. Fig. 9 justifies this statement by demonstrating that the total chemical effect on the S_u^o reduction is not more than 17%. Similarly, the T_{adb} drops linearly with increasing diluent level, as shown in Fig. 10, because the dilution and thermal-diffusion effects (combined) are responsible for 98–100% of the decrease in the T_{adb} due to the diluent addition. The very small remaining percentages of the decrease in the T_{adb} can be almost completely attributed to the chemical effect due to the direct participation of the dilution mixture components in elementary reactions, which disappear at high diluent levels (30–40%).

Detailed sensitivity analysis is performed in order to identify the essential reactions for the S_u^o prediction and point out the possible optimization targets for better S_u^o predictions. Normalized sensitivity coefficients presented in Fig. 11 for the eight most significant elementary reactions for H_2/air combustion suggests that the bimolecular reactions of $H + O_2 \leftrightarrow O + OH$, $OH + H_2 \leftrightarrow H + H_2O$, and $HO_2 + H \leftrightarrow 2OH$ promote the S_u^o most with their large positive sensitivity coefficients. On the other hand, chain terminating reactions of $H + O_2 + M \leftrightarrow HO_2 + M$ and $H + OH + M \leftrightarrow H_2O + M$ inhibit the H_2/air combustion and hinder the S_u^o most with their large negative sensitivity coefficients by competing for H and OH radicals with the above-mentioned bimolecular reactions, which are primarily responsible for active radical production. Therefore, third-body reactions are very important in H_2/oxidizer chemistry and can become more important than bimolecular reactions at high pressures and dilution ratios, as shown in Fig. 11, which justifies the results presented in Fig. 9.

Among the eight most significant elementary reactions shown in Fig. 11, the dilution mixture components (N_2 and H_2O) can participate in third-body reactions of $H + O_2 + M \leftrightarrow HO_2 + M$ and $H + OH + M \leftrightarrow H_2O + M$. The third-body collision efficiency of N_2 is very low while H_2O has very high third-body collision efficiencies for these reactions. Therefore, it can be concluded that H_2O is mainly responsible for the chemical effect of the dilution mixture. Furthermore, tested chemical mechanisms have quite different third-body collision efficiencies for H_2O for these third-body reactions. This together with their different rates for the elementary reactions in Fig. 11 may be some of the sources for the different predictions of S_u^o between mechanisms, particularly at high dilution ratios.

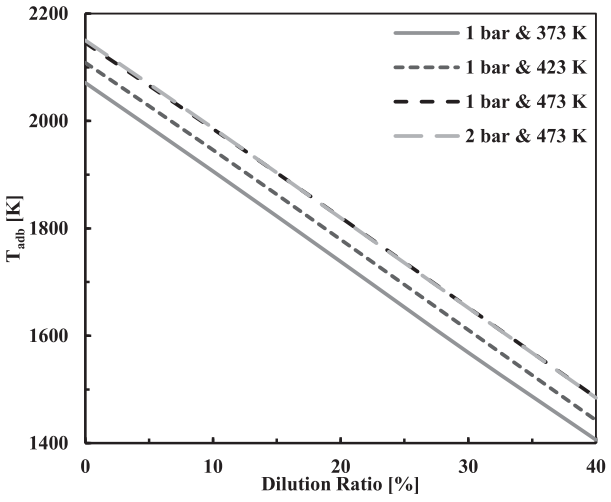

Fig. 10 – Numerical T_{adb} results at 1–2 bar, 373–473 K, 0–40% diluent levels, and $\varphi = 0.7$.

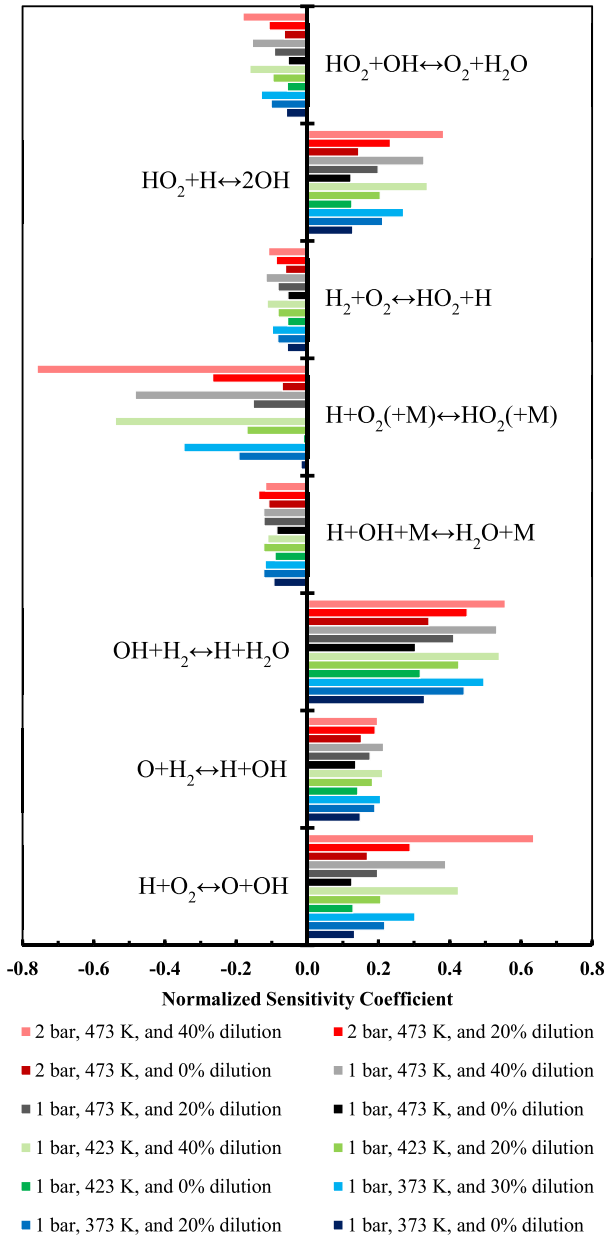

Fig. 11 – Results of detailed sensitivity analyses with respect to the S_u^o.

Conclusions

With increased interest in carbon-free energy production, H_2-fired sequential stage combustors are getting more attention for ground-based power gas turbine engines. Although axial fuel staging provides significant emissions, fuel, and operational flexibilities [1–4], hot (mostly inert) combustion residuals passing onto the secondary stage from the primary stage change the flame reactivity, flame stability, and combustion stability in the secondary burner system [10]. Therefore, it is essential to examine these changes in order to achieve safe (stable), carbon free, and efficient gas turbine engine operation, yet studies investigating the dilution effect of actual main combustion residuals of H_2/air mixtures on fundamental combustion characteristics of H_2/air flames are very scarce.

The overall goal of this study is to advance understanding of combustion and flame characteristics of a secondary burner system for a H_2-fired sequential two-stage combustor. In order to achieve this goal, the effects of actual main residuals of H_2/air combustion (a mixture of 65% N_2 + 35% H_2O by mole) on the S_u^o and L_b of H_2/air mixtures are investigated because the S_u^o and L_b are often associated with the reactivity, exothermicity, and essential flame/combustion stability characteristics of a combustible mixture [14–16]. The S_u^o and L_b of H_2/air mixtures are examined through spherically expanding flame experiments at constant pressure and chemical kinetic analyses at 1–2 bar, 373–473 K, $\varphi = 0.7$, and dilution ratios of 0–40%.

Results of experimental measurements and computational simulations show that the S_u^o increases with increasing unburned gas temperature mainly due to boosted dissociation reactions and greater expansion ratios at elevated temperatures, among which the former effect is more dominant. The S_u^o decreases with increasing initial pressure primarily because of reduced active radicals, which is a result of the increased reaction rate of $H + O_2 + M \leftrightarrow HO_2 + M$ at elevated pressures. The S_u^o and T_{adb} drop with increasing dilution ratio because of lowered H_2/air concentration within the reactants, altered thermodynamic properties of the reactants due to diluent addition, and participation of the dilution mixture components in elementary chemical reactions. The decreases in the S_u^o and T_{adb} due to increasing dilution ratio are almost linear because the dilution and thermal-diffusion effects of the diluent mixture (combined) are responsible for 87–91% of the decrease in the S_u^o and 98–100% of the decrease in the T_{adb}.

Detailed sensitivity analyses highlight the significance of third-body reactions especially at high pressures and dilution ratios because some of them vigorously compete for H and OH radicals with the bimolecular reactions $H + O_2 \leftrightarrow O + OH$, $OH + H_2 \leftrightarrow H + H_2O$, and $HO_2 + H \leftrightarrow 2OH$, which promote the S_u^o most. Special attention should be paid to the chain terminating reactions $H + O_2 + M \leftrightarrow HO_2 + M$ and $H + OH + M \leftrightarrow H_2O + M$ due to their large negative sensitivity coefficients and the very high third-body collision efficiencies of H_2O in these reactions.

The measured L_b values are negative except for very low diluent levels (≤10%) at 1 bar, which implies that the lean H_2/air flames tested in the present study are mostly subject to the thermal diffusive instabilities. While the L_b increases with increasing initial temperature at high diluent levels (>20%), the temperature effect on the L_b at low dilution ratios (≤20%) is generally inappreciable. Furthermore, the hydrodynamic instabilities are promoted at high temperatures as intensified reaction rates lessen the laminar flame thickness. At low dilution ratios (≤20%), the L_b decreases with increasing initial pressure, but there is little influence of pressure on the L_b at higher diluent levels (≥30%). An increase in the combustion pressure leads to a reduction in the flame thickness and therefore intensifies the hydrodynamic instabilities, which is the primary reason for the cellular formation on the H_2 flame surface at 2 bar.

The L_b values of H_2/air mixtures generally decrease with increasing dilution ratio. The dilution effect on the L_b is more complex than the one on the S_u^o because the S_u^o is mainly affected by the T_{adb} change, which is linear, whereas the changes in the L_b are mostly governed by the variation in the thermal/heat and mass diffusivities, i.e. the thermal-diffusion effect. Addition of the dilution mixture into H_2/air mixtures alters their thermal/heat and mass diffusivities and therefore, the Lewis number of the H_2/air mixtures decreases, as does L_b because the Lewis number can be related to the flame response to stretch, i.e. L_b. Addition of the dilution mixture to the reactants increases the H_2 laminar flame thickness and lowers the Darrieus-Landau instability effects.

Lastly, the comparison of experimental measurement results with numerical S_u^o predictions obtained with the NUI Galway-H_2 [58], San Diego [59], HP-Mech [60], Princeton-H_2 [61], Vrije-H_2 [62], and USC-H_2 [63] chemical mechanisms shows that all investigated kinetic models capture the general/overall trend of the experimental results adequately. However, the San Diego [59] and HP-Mech [60] mechanisms suffer from over-predictions (up to 21%) at low/non dilution ratios. Among the tested kinetic mechanisms, the USC-H_2 [63] shows the best agreement with the experimental results whereas the San Diego [59] has the poorest agreement with measurements. The NUI Galway-H_2 [58] predictions are very close to the ones from the USC-H_2 [63]. Similarly, the Princeton-H_2 [61] and Vrije-H_2 [62] predict almost identical S_u^o values, which are more consistent with experimental data at high dilution ratios (≥20%).

Declaration of competing interest

The authors declare that they have no known competing financial interests or personal relationships that could have appeared to influence the work reported in this paper.

Acknowledgements

This material is based upon work partially supported by the National Science Foundation under Grant No. 2129229. The authors would like to thank Yen-Cheng Wang, David Knapp, Andrew Dolenga, and Jianyang Tang for their assistance with measurements, image processing, and numerical analysis.

Appendix A. Supplementary data

Supplementary data to this article can be found online at https://doi.org/10.1016/j.ijhydene.2021.12.217.

REFERENCES

[1] Pennell DA, Bothien MR, Ciani A, Granet V, Singla G, Thorpe S, Wickstroem A, Oumejjoud K, Yaquinto M. An introduction to the Ansaldo GT36 constant pressure sequential combustor. ASME Turbo Expo 2017:GT2017–64790. https://doi.org/10.1115/GT2017-64790.

[2] Karim H, Natarajan J, Narra V, Cai J, Rao S, Kegley J, Citeno J. Staged combustion system for improved emissions operability & flexibility for 7HA class heavy duty gas turbine engine. ASME Turbo Expo 2017:GT2017–63998. https://doi.org/10.1115/GT2017-63998.

[3] Poyyapakkam M, Wood J, Mayers S, Ciani A, Guethe F, Syed K. Hydrogen combustion within a gas turbine reheat combustor. ASME Turbo Expo 2012:GT2012–69165. https://doi.org/10.1115/GT2012-69165.

[4] Zheng X, Xiong Y, Lei F, Deng C, Zhang Z, Xiao Y. Experimental study on the emissions characteristics of a premixed axial-fuel-staged model combustor. J Eng Gas Turbines Power 2020;142(3):031002. https://doi.org/10.1115/1.4045519.

[5] Winkler D, Geng W, Engelbrecht G, Stuber P, Knapp K, Griffin T. Staged combustion concept for gas turbines. J Glob Power Propuls Soc 2017;1:184–94. https://doi.org/10.22261/JGPPS.CVLCX0.

[6] Ciani A, Bothien MR, Bunkute B, Wood JP, Früchtel G. Superior fuel and operational flexibility of sequential combustion in Ansaldo energia gas turbines. J Glob Power Propuls Soc 2019;3:630–8. https://doi.org/10.33737/jgpps/110717.

[7] Schulz O, Noiray N. Combustion regimes in sequential combustors: flame propagation and autoignition at elevated temperature and pressure. Combust Flame 2019;205:253–68. https://doi.org/10.1016/j.combustflame.2019.03.014.

[8] Mishra DP. Fundamentals of combustion. Prentice-Hall Of India Pvt. Limited; 2008.

[9] Goh E, Sirignano M, Li J, Nair V, Emerson B, Lieuwen T, Seitzman J. Prediction of minimum achievable NOx levels for fuel-staged combustors. Combust Flame 2019;200:276–85. https://doi.org/10.1016/j.combustflame.2018.11.027.

[10] Duva BC, Wang Y, Chance LE, Toulson E. Laminar flame characteristics of sequential two-stage combustion of premixed methane/air flames. J Eng Gas Turbines Power 2020;143. https://doi.org/10.1115/1.4048450.

[11] Khosravy el_Hossaini M. Review of the new combustion technologies in modern gas turbines. IntechOpen; 2014. https://doi.org/10.5772/54403.

[12] Bothien MR, Ciani A, Wood JP, Fruechtel G. Sequential combustion in gas turbines: the Key Technology for burning high hydrogen contents with low emissions. ASME Turbo Expo 2019:GT2019–90798. https://doi.org/10.1115/GT2019-90798.

[13] The gas turbine industry's commitments to drive the transition to renewable-gas power generation. EUTurbines; 2019. https://powertheeu.eu/.

[14] Wu CK, Law CK. On the determination of laminar flame speeds from stretched flames. Symp Combust Proc 1985;20:1941–9. https://doi.org/10.1016/S0082-0784(85)80693-7.

[15] Turns SR. An introduction to combustion: concepts and applications. New York: McGraw-Hill; 2012.

[16] Bradley D, Gaskell PH, Gu X. Burning velocities, markstein lengths, and flame quenching for spherical methane-air flames: a computational study. Combust Flame 1996;104:176–98. https://doi.org/10.1016/0010-2180(95)00115-8.

[17] Egolfopoulos FN, Hansen N, Ju Y, Kohse-Höinghaus K, Law CK, Qi F. Advances and challenges in laminar flame experiments and implications for combustion chemistry. Prog Energy Combust Sci 2014;43:36–67. https://doi.org/10.1016/j.pecs.2014.04.004.

[18] Tse SD, Zhu DL, Law CK. Morphology and burning rates of expanding spherical flames in H2/O2/inert mixtures up to 60 atmospheres. Proc Combust Inst 2000;28:1793–800. https://doi.org/10.1016/S0082-0784(00)80581-0.

[19] Lu X, Hu E, Li X, Ku J, Huang Z. Non-monotonic behaviors of laminar burning velocities of H2/O2/He mixtures at elevated pressures and temperatures. Int J Hydrogen Energy 2017;42:22036–45. https://doi.org/10.1016/j.ijhydene.2017.07.055.

[20] Gong Y, Huang X, Deng J, Li L. Experimental and numerical study on combustion characteristics of super lean H2–O2 premixed laminar flame in argon atmosphere. Int J Hydrogen Energy 2020;45:21956–68. https://doi.org/10.1016/j.ijhydene.2020.05.179.

[21] Liu DDS, MacFarlane R. Laminar burning velocities of hydrogen-air and hydrogen-air-steam flames. Combust Flame 1983;49:59–71. https://doi.org/10.1016/0010-2180(83)90151-7.

[22] Koroll GW, Mulpuru SR. The effect of dilution with steam on the burning velocity and structure of premixed hydrogen flames. Symp Combust Proc 1988;21:1811–9. https://doi.org/10.1016/S0082-0784(88)80415-6.

[23] Aung KT, Hassan MI, Faeth GM. Effects of pressure and nitrogen dilution on flame/stretch interactions of laminar premixed H2/O2/N2 flames. Combust Flame 1998;112:1–15. https://doi.org/10.1016/S0010-2180(97)81753-1.

[24] Kwon OC, Faeth GM. Flame/stretch interactions of premixed hydrogen-fueled flames: measurements and predictions. Combust Flame 2001;124:590–610. https://doi.org/10.1016/S0010-2180(00)00229-7.

[25] Lamoureux N, Djebaïli-Chaumeix N, Paillard CE. Laminar flame velocity determination for H2–air–He–CO2 mixtures using the spherical bomb method. Exp Therm Fluid Sci 2003;27:385–93. https://doi.org/10.1016/S0894-1777(02)00243-1.

[26] Qiao L, Kim CH, Faeth GM. Suppression effects of diluents on laminar premixed hydrogen/oxygen/nitrogen flames. Combust Flame 2005;143:79–96. https://doi.org/10.1016/j.combustflame.2005.05.004.

[27] Hu E, Huang Z, He J, Jin C, Miao H, Wang X. Measurement of laminar burning velocities and analysis of flame stabilities for hydrogen-air-diluent premixed mixtures. Chin Sci Bull 2009;54:846–57. https://doi.org/10.1007/s11434-008-0584-y.

[28] Hermanns RTE, Konnov AA, Bastiaans RJM, de Goey LPH. Laminar burning velocities of diluted hydrogen-oxygen-nitrogen mixtures. Energy Fuels 2007;21:1977–81. https://doi.org/10.1021/ef060553g.

[29] Paidi SK, Bhavaraju A, Akram M, Kumar S. Effect of N2/CO2 dilution on laminar burning velocity of H2–air mixtures at high temperatures. Int J Hydrogen Energy 2013;38:13812–21. https://doi.org/10.1016/j.ijhydene.2013.08.024.

[30] Santner J, Dryer FL, Ju Y. The effects of water dilution on hydrogen, syngas, and ethylene flames at elevated pressure. Proc Combust Inst 2013;34:719–26. https://doi.org/10.1016/j.proci.2012.06.065.

[31] Li H, Li G, Sun Z, Zhou Z, Li Y, Yuan Y. Fundamental combustion characteristics of lean and stoichiometric hydrogen laminar premixed flames diluted with nitrogen or carbon dioxide. J Eng Gas Turbines Power 2016;138:111501. https://doi.org/10.1115/1.4032315.

[32] Yang S, Yang X, Wu F, Ju Y, Law CK. Laminar flame speeds and kinetic modeling of H2/O2/diluent mixtures at sub-atmospheric and elevated pressures. Proc Combust Inst 2017;36:491–8. https://doi.org/10.1016/j.proci.2016.06.122.
[33] Lyu Y, Qiu P, Liu L, Yang C, Sun S. Effects of steam dilution on laminar flame speeds of H2/air/H2O mixtures at atmospheric and elevated pressures. Int J Hydrogen Energy 2018;43:7538–49. https://doi.org/10.1016/j.ijhydene.2018.02.065.
[34] Lu X, Hu E, Kokjohn S, Gao Q, Yin G, Zeng K, Huang Z. Experimental and kinetic study of laminar flame characteristics of H2/O2/diluent flame under elevated pressure. Int J Hydrogen Energy 2020;45:32508–20. https://doi.org/10.1016/j.ijhydene.2020.08.142.
[35] Duan J, Liu F. Laminar combustion characteristics and mechanism of hydrogen/air mixture diluted with N2 + H2O. Int J Hydrogen Energy 2017;42:4501–7. https://doi.org/10.1016/j.ijhydene.2016.10.071.
[36] Duva BC, Chance LE, Toulson E. Dilution effect of different combustion residuals on laminar burning velocities and burned gas Markstein lengths of premixed methane/air mixtures at elevated temperature. Fuel 2020;267:117153. https://doi.org/10.1016/j.fuel.2020.117153.
[37] Galmiche B, Halter F, Foucher F, Dagaut P. Effects of dilution on laminar burning velocity of premixed methane/air flames. Energy Fuels 2011;25:948–54. https://doi.org/10.1021/ef101482d.
[38] Lefebvre AH, Ballal DR. Gas turbine combustion: alternative fuels and emissions. Taylor & Francis; 2010.
[39] Li J, Yuan L, Mongia HC. Simulation investigation on combustion characteristics in a four-point lean direct injection combustor with hydrogen/air. Appl Sci 2017;7:619. https://doi.org/10.3390/app7060619.
[40] Van TG, Hwang JJ, Kim MK, Ahn KY. Feasibility study of ultra-low NOx Gas turbine combustor using the RML combustion concept. J Mech Sci Technol 2016;30:5749–57. https://doi.org/10.1007/s12206-016-1145-y.
[41] Gotoda H, Nikimoto H, Miyano T, Tachibana S. Dynamic properties of combustion instability in a lean premixed gas-turbine combustor. Chaos 2011;21:013124. https://doi.org/10.1063/1.3563577.
[42] Duva BC, Chance LE, Toulson E. Laminar flame speeds of premixed iso-octane/air flames at high temperatures with CO2 dilution. SAE Int J Adv Curr Pract Mobil 2019;1:1148–57. https://doi.org/10.4271/2019-01-0572.
[43] Duva BC, Wang Y, Chance LE, Toulson E. The effect of exhaust gas recirculation (EGR) on fundamental characteristics of premixed methane/air flames. SAE Technical Paper; 2020. https://doi.org/10.4271/2020-01-0339. 2020-01-0339.
[44] Duva BC, Chance LE, Toulson E. Effect of CO2 dilution on the laminar burning velocities of premixed methane/air flames at elevated temperature. J Eng Gas Turbines Power 2020;142:031014. https://doi.org/10.1115/1.4044641.
[45] Duva BC, Chance LE, Toulson E. The critical lower radius limit approach for laminar flame speed measurement from spherically expanding stretched flames. Exp Therm Fluid Sci 2021;121:110284. https://doi.org/10.1016/j.expthermflusci.2020.110284.
[46] Duva BC, Chance LE, Toulson E. Experimental and numerical investigation of the CO2 dilution effect on laminar burning velocities and burned gas markstein lengths of high/low RON gasolines and isooctane flames at elevated temperatures. Energy Fuels 2020;34:996–1004. https://doi.org/10.1021/acs.energyfuels.9b03854.
[47] Duva BC. Investigation of the dilution effect on laminar flame characteristics in a constant volume combustion chamber. Michigan State University; 2021. Doctoral dissertation, https://www.proquest.com/openview/511ce41a427744be66322ed55de86000/1?pq-origsite=gscholar&cbl=18750&diss=y.
[48] Settles GS. Schlieren and shadowgraph techniques: visualizing phenomena in transparent media. Berlin Heidelberg: Springer; 2001. https://doi.org/10.1007/978-3-642-56640-0.
[49] Markstein GH. Experimental and theoretical studies of flame-front stability. J Aeronaut Sci 1951;18:199–209. https://doi.org/10.2514/8.1900.
[50] Chen Z. On the extraction of laminar flame speed and Markstein length from outwardly propagating spherical flames. Combust Flame 2011;158:291–300. https://doi.org/10.1016/j.combustflame.2010.09.001.
[51] Kelley AP, Law CK. Nonlinear effects in the extraction of laminar flame speeds from expanding spherical flames. Combust Flame 2009;156:1844–51. https://doi.org/10.1016/j.combustflame.2009.04.004.
[52] Ronney PD, Sivashinsky GI. A theoretical study of propagation and extinction of nonsteady spherical flame fronts. J Appl Math 1989;49:1029–46. https://doi.org/10.1137/0149062.
[53] Wu F, Liang W, Chen Z, Ju Y, Law CK. Uncertainty in stretch extrapolation of laminar flame speed from expanding spherical flames. Proc Combust Inst 2015;35:663–70. https://doi.org/10.1016/j.proci.2014.05.065.
[54] Li X, Hu E, Meng X, Peng C, Lu X, Huang Z. Effect of Lewis number on nonlinear extrapolation methods from expanding spherical flames. Combust Sci Technol 2017;189:1510–26. https://doi.org/10.1080/00102202.2017.1305369.
[55] Yu H, Han W, Santner J, Gou X, Sohn CH, Ju Y, Chen Z. Radiation-induced uncertainty in laminar flame speed measured from propagating spherical flames. Combust Flame 2014;161:2815–24. https://doi.org/10.1016/j.combustflame.2014.05.012.
[56] Burke MP, Chen Z, Ju Y, Dryer FL. Effect of cylindrical confinement on the determination of laminar flame speeds using outwardly propagating flames. Combust Flame 2009;156:771–9. https://doi.org/10.1016/j.combustflame.2009.01.013.
[57] Chen Z. On the accuracy of laminar flame speeds measured from outwardly propagating spherical flames: methane/air at normal temperature and pressure. Combust Flame 2015;162:2442–53. https://doi.org/10.1016/j.combustflame.2015.02.012.
[58] O'Connaire M, Curran HJ, Simmie JM, Pitz WJ, Westbrook CK. A comprehensive modeling study of hydrogen oxidation. Int J Chem Kinet 2004;36:603–22. https://doi.org/10.1002/kin.20036.
[59] "Chemical-Kinetic mechanisms for combustion applications," san Diego mechanism web page, Mechanical and aerospace engineering (combustion research), University of California at San Diego. http://combustion.ucsd.edu. [Accessed 13 October 2019]. http://web.eng.ucsd.edu/mae/groups/combustion/mechanism.html.
[60] Yang X, Shen X, Santner J, Zhao H, Ju Y. Princeton HP-mech. http://engine.princeton.edu/mechanism/HP-Mech.html. [Accessed 13 October 2019].
[61] Li J, Zhao Z, Kazakov A, Dryer FL. An updated comprehensive kinetic model of hydrogen combustion. Int J Chem Kinet 2004;36:566–75. https://doi.org/10.1002/kin.20026.
[62] Konnov AA. Yet another kinetic mechanism for hydrogen combustion. Combust Flame 2019;203:14–22. https://doi.org/10.1016/j.combustflame.2019.01.032.
[63] Davis SG, Joshi AV, Wang H, Egolfopoulos F. An optimized kinetic model of H2/CO combustion. Proc Combust Inst 2005;30:1283–92. https://doi.org/10.1016/j.proci.2004.08.252.

[64] Ansys chemkin-pro 17.2. San Diego: ANSYS Reaction Design; 2016.
[65] Mueller MA, Kim TJ, Yetter RA, Dryer FL. Flow reactor studies and kinetic modeling of the H2/O2 reaction. Int J Chem Kinet 1999;31:113–25. https://doi.org/10.1002/(SICI)1097-4601(1999)31:2<113:AID-KIN5>3.0.CO;2-0.
[66] Weydahl T, Poyyapakkam M, Seljeskog M, Haugen N Erland L. Assessment of existing H2/O2 chemical reaction mechanisms at reheat gas turbine conditions. Int J Hydrogen Energy 2011;36:12025–34. https://doi.org/10.1016/j.ijhydene.2011.06.063.
[67] Olm C, Zsély IG, Pálvölgyi R, Varga T, Nagy T, Curran HJ, Turányi T. Comparison of the performance of several recent hydrogen combustion mechanisms. Combust Flame 2014;161:2219–34. https://doi.org/10.1016/j.combustflame.2014.03.006.
[68] Yang S, Yang X, Wu F, Ju Y, Law CK. Laminar flame speeds and kinetic modeling of H2/O2/diluent mixtures at sub-atmospheric and elevated pressures. Proc Combust Inst 2017;36:491–8. https://doi.org/10.1016/j.proci.2016.06.122.
[69] Smith GP, Golden DM, Frenklach M, Moriary NW, Eiteneer B, Goldenberg M, Bowman CT, Hanson RK, Song S, Gardiner WC, Lissianski VV, Qin Z. GRI-Mech 3.0. http://www.me.berkeley.edu/gri_mech/.
[70] Somers KP, Simmie JM, Gillespie F, Conroy C, Black G, Metcalfe WK, Battin-Leclerc F, Dirrenberger P, Herbinet O, Glaude PA, Dagaut P, Togbé C, Yasunaga K, Fernandes RX, Lee C, Tripathi R, Curran HJ. A comprehensive experimental and detailed chemical kinetic modelling study of 2,5-dimethylfuran pyrolysis and oxidation. Combust Flame 2013;160:2291–318. https://doi.org/10.1016/j.combustflame.2013.06.007.
[71] Liu X, Wang H, Zheng Z, Liu J, Reitz RD, Yao M. Development of a combined reduced primary reference fuel-alcohols (methanol/ethanol/propanols/butanols/n-pentanol) mechanism for engine applications. Energy 2016;114:542–58. https://doi.org/10.1016/j.energy.2016.08.001.
[72] Dong C, Zhou Q, Zhang X, Zhao Q, Xu T, Hui S. Experimental study on the laminar flame speed of hydrogen/natural gas/air mixtures. Front Chem Eng China 2010;4:417–22. https://doi.org/10.1007/s11705-010-0515-8.
[73] Kuznetsov M, Kobelt S, Grune J, Jordan T. Flammability limits and laminar flame speed of hydrogen–air mixtures at sub-atmospheric pressures. Int J Hydrogen Energy 2012;37:17580–8. https://doi.org/10.1016/j.ijhydene.2012.05.049.
[74] Krejci MC, Mathieu O, Vissotski AJ, Ravi S, Sikes TG, Petersen EL, Kermon'es A, Metcalfe W, Curran HJ. Laminar flame speed and ignition delay time data for the kinetic modelling of hydrogen and syngas fuel blends. J Eng Gas Turbines Power 2013;135(2):021503. https://doi.org/10.1115/1.4007737.
[75] Beeckmann J, Pitsch H. Laminar burning velocities of spherically expanding hydrogen/air mixtures for temperatures up to 423K at ambient pressure. In: Proceedings of the twenty-sixth international colloquium on the dynamics of explosions and reactive systems; 2017. p. 1175. http://www.icders.org/ICDERS2017/abstracts/ICDERS2017-1175.pdf.
[76] Glassman I, Yetter RA, Glumac NG. Combustion. Academic press; 2014.
[77] Metghalchi M, Keck JC. Laminar burning velocity of propane-air mixtures at high temperature and pressure. Combust Flame 1980;38:143–54. https://doi.org/10.1016/0010-2180(80)90046-2.
[78] Lasdon LS, Waren AD, Jain A, Ratner M. Design and testing of a generalized reduced gradient code for nonlinear programming. ACM Trans Math Software 1978;4:34–50. https://doi.org/10.1145/355769.355773.
[79] Bradley D, Harper CM. The development of instabilities in laminar explosion flames. Combust Flame 1994;99(3):562–72. https://doi.org/10.1016/0010-2180(94)90049-3.
[80] Matalon M. Flame dynamics. Proc Combust Inst 2009;32(1):57–82. https://doi.org/10.1016/j.proci.2008.08.002.
[81] Matalon M. The Darrieus–Landau instability of premixed flames. Fluid Dynam Res 2018;50(5):051412. https://doi.org/10.1088/1873-7005/aab510.
[82] Manton J, von Elbe G, Lewis B. Nonisotropic propagation of combustion waves in explosive gas mixtures and the development of cellular flames. J Chem Phys 1952;20(1):153–7. https://doi.org/10.1063/1.1700159.
[83] Duva BC, Wang YC, Chance LE, Toulson E. Correlations for the laminar burning velocity and burned gas Markstein length of methane-air mixtures diluted with flue gases at high temperatures and pressures. Fuel 2020;281:118721. https://doi.org/10.1016/j.fuel.2020.118721.
[84] Zahedi P, Yousefi K. Effects of pressure and carbon dioxide, hydrogen and nitrogen concentration on laminar burning velocities and NO formation of methane-air mixtures. J Mech Sci Technol 2014;28:377–86. https://doi.org/10.1007/s12206-013-0970-5.
[85] Chan YL, Zhu MM, Zhang ZZ, Liu PF, Zhang DK. The effect of CO2 dilution on the laminar burning velocity of premixed methane/air flames. Energy Proc 2015;75:3048–53. https://doi.org/10.1016/j.egypro.2015.07.621.